# Mapping Co-regulatory Interactions among Ligand Binding sites in RyR1

Venkat R. Chirasani[1,2], Konstantin I. Popov[2], Gerhard Meissner[2], and Nikolay V. Dokholyan[1*]

[1]Departments of Pharmacology, and Biochemistry and Molecular Biology, Penn State College of Medicine, Hershey, PA 17033 and [2]Department of Biochemistry and Biophysics, University of North Carolina, Chapel Hill, NC 27599.

Running title: *Allosteric coupling among RyR1 ligand binding sites*

*Corresponding author: Departments of Pharmacology, and Biochemistry and Molecular Biology, Penn State College of Medicine, Hershey, PA 17033-0850, Telephone: (717) 531-5177, E-mail: dokh@psu.edu.

**Keywords:** Ryanodine receptor, allosteric coupling, percolation theory, computational analysis, single channel measurements, and allosteric interactions.

**Abstract**

Ryanodine receptor 1 (RyR1) is an intracellular calcium ion ($Ca^{2+}$) release channel required for skeletal muscle contraction. Although cryo-electron microscopy identified binding sites of three coactivators $Ca^{2+}$, ATP and caffeine (CFF), the mechanism of co-regulation and synergy of these activators is unknown. Here, we report allosteric connections among the three ligand binding sites and pore region in (i) $Ca^{2+}$ bound-closed, (ii) ATP/CFF bound- closed, (iii) $Ca^{2+}$/ATP/CFF bound-closed, and (iv) $Ca^{2+}$/ATP/CFF bound-open RyR1 states. We identified two dominant networks of interactions that mediate communication between the $Ca^{2+}$ binding site and pore region in $Ca^{2+}$ bound-closed state, which partially overlapped with the pore communications in ATP/CFF bound-closed RyR1 state. In $Ca^{2+}$/ATP/CFF bound-closed and -open RyR1 states, co-regulatory interactions were analogous to communications in the $Ca^{2+}$ bound-closed and ATP/CFF bound- closed states. Both ATP- and CFF- binding sites mediate communication between the $Ca^{2+}$ binding site and the pore region in $Ca^{2+}$/ATP/CFF bound - open RyR1 structure. We conclude that $Ca^{2+}$, ATP, and CFF propagate their effects to the pore region through a network of overlapping interactions that mediate allosteric control and molecular synergy in channel regulation.

**Statement of Significance**

Ryanodine receptors (RyRs) are a group of $Ca^{2+}$ channels that bind to endogenous and exogenous modulators to regulate $Ca^{2+}$ release through closed-to-open gating transitions. Recent advances in single-particle cryo-electron microscopy (cryo-EM) have captured RyR1 in multiple states and provide insights into RyR1 regulation by endogenous activators $Ca^{2+}$ and ATP and exogenous activator caffeine (CFF). Despite the high-resolution structural data available for

RyR1, the allosteric mechanism of RyR1 gating is not well understood. In this study, we used a graph-theoretical approach to predict the allosteric networks of interactions among various co-activators in RyR1 that control opening/closing of the pore region. Such synergistic coordination appears to be necessary for channel regulation by multiple activators, which includes co-regulation among various activators in RyR1 that regulate the closed−to−open gating transitions. The findings may assist in the design of strategies to control allosteric regulation of RyR1. Understanding of allosteric coupling among the ligand sites and pore region in RyR1 may enable the design of advanced therapeutics for several debilitating diseases.

**Introduction**

RyRs are homo-tetrameric intracellular $Ca^{2+}$ channels that mediate the rapid release of $Ca^{2+}$ ions from the sarcoplasmic reticulum (SR) into the cytoplasm for muscle contraction (1–5). RyRs are the largest known ion channels with molecular mass of ~2.2 megadaltons comprised of four 560-kDa RyR subunits and four ~12-kDa FK506 binding protein subunits. There are three RyR isoforms in mammalian cells: RyR1 in skeletal muscle, RyR2 in heart muscle, and RyR3 in many tissues but in lower concentrations. RyR1 is controlled by direct interaction with $Ca_v1.1$ voltage-gated $Ca^{2+}$ channels, and by $Ca^{2+}$ through an unknown mechanism (3, 6, 7). In contrast, influx of extracellular $Ca^{2+}$ through voltage-gated $Ca^{2+}$ channels activate RyR2 and RyR3 and triggers the release of $Ca^{2+}$ by $Ca^{2+}$-induced $Ca^{2+}$ release mechanism. Endogenous modulators, $Ca^{2+}$, ATP, $Mg^{2+}$, and calmodulin along with the exogenous effectors, CFF and Ryanodine regulate the function of RyR1 (3). Despite the presence of activator binding sites in close proximity to the pore region of RyRs and the possibility of allosteric communications within the channels, the mechanism of allosteric regulation is still unclear (8–12).

Recent advances in single-particle cryo-electron microscopy (cryo-EM) have captured RyR1 in multiple states that implicate $Ca^{2+}$, ATP and CFF as key activators in RyR1 regulation (8–10, 13–17). High resolution cryo-EM structures emphasized binding of $Ca^{2+}$, ATP, and CFF as trigger for local and global structural changes in RyR1 to induce channel opening (10, 17). Mutagenesis and single-channel recordings have revealed the role of $Ca^{2+}$ binding site residues Glu-3893, Glu-3967, and Thr-5001 in $Ca^{2+}$-dependent activation of RyR1 (18). Further, Murayama et al demonstrated that Trp-4716 in the CFF-binding pocket regulate $Ca^{2+}$ sensitivity by controlling the structure of the $Ca^{2+}$-binding site (19). Additionally, recent computational studies suggested that allosteric gating of RyR1 is influenced by extensive structural changes in the RyR1 peripheral and central domains (11, 12, 17). While the cryo-EM structures and experimental studies provide insights into ligand binding and structural states, the allosteric mechanisms that couple and synergize communication among the ligand binding sites and pore region in RyR1 are not well understood.

In this study we present the structural basis for allosteric control of $Ca^{2+}$- binding site and pore region in open and closed RyR1 channels. We also show how binding of ATP and CFF alters the allosteric network and affects $Ca^{2+}$-free and $Ca^{2+}$-occupied channel activities. Conformational changes related to channel opening or closing appear to alter the allosteric network. Synergistic interactions among the three activators $Ca^{2+}$, ATP and CFF propagate their effects to the pore region through a network of connecting amino acid residues.

## Materials and Methods

*Mapping allosteric communication in different functional states of RyR1*

We analyzed the cryo-EM structures of different RyR1 states: $Ca^{2+}$ bound-closed RyR1 (PDB ID: 5T15), ATP/CFF bound-closed RyR1 (PDB ID: 5TAP), $Ca^{2+}$/ATP/CFF bound-closed RyR1 (PDB ID: 5TAQ), and $Ca^{2+}$/ATP/CFF bound-open RyR1 (PDB ID: 5TAL) to map allosteric interactions among the activator binding sites using our recently developed methodology (20–23). We chose $Ca^{2+}$, ATP, CFF Gly-4934 the channel gating residue (24) to annotate the pore region. The detailed methodology of allosteric interaction prediction among the chosen sites is described below.

*Construction of protein graphs.*

Graph representations G(N, E) were constructed for each channel state, where $n_i$ are nodes corresponding to each protein residue, $e_{ij}$ are edges connecting each pair of nodes *i* and *j* and *i,j*=1…N corresponds to residue number, where N is the protein size (25). To further incorporate structural information of the protein, we assigned weight ($e_{ij}$) for each graph edge as shown below.

$$e_{ij} = \frac{w_{ij}}{max\left(w_{ij}\right)} \qquad [1]$$

and

$$w_{ij} = \sum_{k,l}^{a_i a_j} H\left(r_0 - \left|\vec{r}_k - \vec{r}_l\right|\right) \qquad [2]$$

where H(x) is a Heaviside step function and $r_0$ =4 Å is a cutoff distance. The summation is over all pairs of heavy atoms $a_i$ and $a_j$ (amino acid atoms excluding hydrogens, i.e. C, O, N, S) in two residues of the protein i and j. The parameter $\left|\vec{r}_k - \vec{r}_l\right|$ denotes pair distance between two heavy atoms in residues *i* and j. Equation [2] represents a simplified method to quantify the strength of

interaction between amino acid residues in the protein. In this case, $w_{ij}$ favors edges of the graph, which connect nodes $n_i$ and $n_j$ corresponding to stronger interacting residues of the protein i and j. If two residues have a distance between any of their atoms greater than $r_0$, corresponding edge weight for those residues was set as zero. The detailed methodology on construction and evaluation of protein structure graphs based on edge weights can be found in the ref: (23).

*Shortest pathway and paths clustering.*

To map allosteric interactions between two residues, the shortest paths between two nodes on the graph were identified (either ligand–ligand or ligand–Gly-4934). Yen's algorithm was used to compute rank-ordered loop-less optimal interactions (26). For each iteration Yen's algorithm uses Dijkstra algorithm (26, 27), which calculates the optimal connection responsible for propagation of communication through the network. The product of edge weights along the path was used as a metrics to quantify communication strength along the pathway:

$$Q_k = \prod_{ij \in \{path\,k\}} e_{ij}, \qquad [3]$$

Representative allosteric interactions were predicted by hierarchical clustering of the top 10,000 optimal communication pathways using the measure for the dissimilarity between them,

$$d_{lm} = max\left(n_l, n_m\right) - n_{lm} \quad [4]$$

where, $n_l$ and $n_m$ denote the number of nodes in path $l$ and $m$, and $n_{lm}$ ($0 \le n_{lm} \le min\left(n_l, n_m\right)$) is the number of common nodes in both paths. Clustering according to this distance allows to combine pathways with minimal deviations from each other (large $n_{lm}$). After each step of clustering, we

consider that the representative path carries the allosteric communication equal to the sum of those carried by all merged pathways. There are several ways to choose the cutoff for hierarchical clustering (28). The detailed methodology on construction and evaluation of protein structure graphs based on edge weights can be found in the ref: (23).

In this work, we observed that the allosteric networks always had several strongest distinctive pathways that were carried through the clustering procedure and were always becoming representative interactions in the end of clustering. Based on this observation, for simplicity of representation we show and analyzed only top five pathways (Figs. 2–5). We performed allosteric interaction analyses on tetrameric rather than monomeric conformations of RyR1 in different functional states as stated above. All structural figures were rendered using PyMOL (The PyMOL Molecular Graphics System, Version 2.0 Schrödinger, LLC).

**Results**

Cryo-EM structures of RyR1 solved in different functional states have identified the binding sites for channel activators $Ca^{2+}$, ATP and CFF at inter-domain interfaces of the C-terminal domain (CTD) (Fig. 1) (10). Comparison of cryo-EM density maps in the presence of $Ca^{2+}$ but without ATP/CFF, and in the presence of ATP/CFF without $Ca^{2+}$ indicate variations in densities of core solenoid (residues 3667-4174) and CTD (residues 4957-5037) of RyR1, that suggest the synergy in the activation of RyR1 by $Ca^{2+}$ and ATP/CFF (10). Co-localization of ATP, CFF, and $Ca^{2+}$ binding sites at interfaces of the CTD suggests allosteric communication between these binding sites during channel opening and/or closing.

To establish an allosteric network among $Ca^{2+}$, ATP, and CFF binding sites during channel activation, allosteric interaction analysis was performed on tetrameric conformations of four

structures: $Ca^{2+}$ bound-closed RyR1 (PDB ID: 5T15), ATP/CFF bound-closed RyR1 (PDB ID: 5TAP), $Ca^{2+}$/ATP/CFF bound-closed RyR1 (PDB ID: 5TAQ), and $Ca^{2+}$/ATP/CFF bound-open RyR1 (PDB ID: 5TAL). A graph-theoretical approach was used to depict allosteric interactions among the chosen ligand binding sites in RyR1 structures by comparing relative allosteric communication transmitted through each residue in a specific sequence of interactions. The bar charts specific to each pathway illustrate the amount of relative allosteric communication transmitted by each residue specific to that pathway and subsequently highlight allosteric hot spot residues crucial for the communication (Figs. 2–5). Thus, communication between ligand binding sites and pore region was predicted with maximal contribution to the allosteric couplings.

*$Ca^{2+}$ binding site to pore communication propagate through unoccupied CFF-binding site in $Ca^{2+}$ bound- closed RyR1.*

The binding site for $Ca^{2+}$ is constituted by side chains Glu-3893 and Glu-3967 (core solenoid) and the backbone of the CTD residue Thr-5001 (Fig. 1B and Fig. S1). Cryo-EM data indicate the $Ca^{2+}$ binding site is situated in close proximity to the ATP and CFF binding sites and the three sites are likely coupled to regulate binding or release of $Ca^{2+}$ either directly or indirectly (Fig. 1A) (10). The influence of unoccupied CFF and ATP binding sites on $Ca^{2+}$ to pore communication was determined by analyzing $Ca^{2+}$ only bound-closed RyR1 structure (PDB ID: 5T15) using percolation theory and computational modeling techniques. The allosteric network of the $Ca^{2+}$ bound-closed RyR1 structure contained two main $Ca^{2+}$ binding site pore interactions, a primary connection propagating through CFF binding site residues Tyr-5014 and Glu-4239, and a secondary one independent of CFF and ATP binding sites (Fig. 2). The primary

interactions initiated from $Ca^{2+}$-binding pocket residue Thr-5001 progressed through CTD residues Thr-5004, Trp-5011, Glu-5007 to CFF binding site residues Tyr-5014 (CTD) and Glu-4239 (TaF domain). Allosteric communication was further propagated via hydrophobic interactions between Glu-4239 and Phe-4237 (TaF domain), aromatic interactions between Phe-4237 and Phe-4217 (TaF domain), and hydrophobic interactions among TaF domain residues Phe-4217, Val-4221, Asn-4223, and S6c helix residues Gln-4946, Arg-4944, Asp-4938, and Ile-4937 (constriction site of the $Ca^{2+}$ bound-closed RyR1 channel) (10, 14, 30). The secondary interactions also initiated from $Ca^{2+}$ binding pocket residue Thr-5001 but progressed along CTD residues Asp-4999, Lys-4998, Tyr-4994, and Met-4993 through covalent or hydrophobic interactions (Fig. 2). Allosteric signaling advanced from the CTD to the TaF domain through tightly packed Ile-4242 and Met-4993 sidechains. As observed in the primary interaction, the TaF domain residues: Phe-4237, Phe-4217, Val-4221, Asn-4223 along with the S6c helix residues: Gln-4946, Arg-4944, Asp-4938 and Ile-4937 mediated the signal to the pore region. Thus, in $Ca^{2+}$ bound-closed RyR1, $Ca^{2+}$ binding site communicate to the pore region via the CTD, the TaF, and the S6c domains. Interestingly, the $Ca^{2+}$ - pore interactions propagated through the unoccupied CFF binding site but evade the unoccupied ATP binding site.

*ATP- and CFF- binding sites communicate with the pore region in ATP/CFF bound-closed RyR1.*

Previous studies suggest that ATP and CFF activate RyR1 in the absence or presence of $Ca^{2+}$ (18). In this work, a potential network of allosteric connections among ATP-,CFF- binding sites, and pore region in the absence of $Ca^{2+}$ was investigated using the ATP/CFF bound-closed RyR1 (PDB ID: 5TAP) (Fig. 3). Three major interactions were predicted involving polar, aromatic, and

non-covalent residues in the CTD, TaF, S2S3, and S6c helix domains (Fig. 3). The major pathway initiated from the CFF binding site residue Glu-4239 resembled allosteric interactions in $Ca^{2+}$ bound-closed RyR1 structure that connected the TaF domain residues Phe-4237, Phe-4217, Phe-4219, and S6c helix residues Gln-4947, Arg-4944, Asp-4938 and Ile-4937. A second interaction originated from the CFF binding site residue Trp-4716 proceeded through the S2S3 domain residues Lys-4675, Phe-4671 and Lys-4672 and merged with the major pathway. A third pathway initiated from the CFF site residue Ile-4996 passed through ATP binding site residue Met-4954 and merged with previously solved pathways at S6c residue: Gln-4947 (Fig. 3). Finally, the merged pathways passed through the CTD residues: Leu-4992, Met-4989, Ala-4986, Leu-4985 and S6c residues: Met-4954, Glu-4955, Lys-4951, Glu-4948, Gln-4947, Arg-4944, Asp-4938 and communicated the pore region (Figs. 3, S1, S4A). Altogether, three different networks of allosteric interactions originate from the CFF binding site progressed through the activation module to communicate with the pore region. During the progression of the allosteric signal from the CFF-binding site, while one pathway interacted the ATP-binding site, remaining two pathways avoided it.

*Three diverse networks of allosteric interactions communicate the effects of $Ca^{2+}$ binding to the pore region in the $Ca^{2+}$/ATP/CFF bound-closed RyR1 structure.*

Three sets of allosteric interactions predicted in the $Ca^{2+}$/ATP/CFF bound-closed RyR1 structure (PDB ID: 5TAQ) involve mostly polar and aromatic residues to mediate the communication between the $Ca^{2+}$ binding site and pore region. While two networks of interactions passed through the CFF- (Fig. 4, Fig. S2A, and Fig. S5A) and ATP- binding sites (Fig. 4, Fig. S3A, and Fig. S6A), a third network bypassed these two binding sites (Fig. 4). The

three predicted allosteric networks of interactions between the $Ca^{2+}$ binding site and pore region are as follows: (a) CTD residues Thr-5001, Asp-4999, Lys-4998, Ile-4996 (CFF binding site), TaF residues Glu-4239 (CFF binding site), Phe-4237, Phe-4217, Phe-4219, and S6c residues Gln-4946, Glu-4942, Asp-4938, Ile 4937, Gly-4934, (b) Core Solenoid (CSol) residue Glu-3970, CTD residues Glu-5002, Asn-5003, Lys-4998, Tyr-4994, Met-4993, TaF residues Ile-4242, Phe-4237, Phe-4217, Phe-4219, and S6c residues Gln-4946, Glu-4942, Asp-4938*, Ile-4937*, Gly-4934, and (c) Core Solenoid residue Glu-3970, CTD residues Glu-5002, Asn-5003, Lys-4998, Tyr-4994, Phe-4990, Asn-4987, Asn-4984, and S6c residues Met-4954 (ATP binding site), Lys-4951, Glu-4948, Asp-4945, Arg-4944, Asp-4938*, Ile-4937* and Gly-4934. It is worth mentioning here that the allosteric signal in network-b and network-c passed from S6c helix in one monomer to S6c helix in another monomer before terminating at the pore region (denoted by * above) (Fig. 4). Interestingly, the TaF domain residues Glu-4239, Phe-4237, Phe-4217 and Arg-4215 provided direct communication between the ATP- and CFF- binding sites in $Ca^{2+}$/ATP/CFF bound-closed RyR1 (Fig. 4 and Fig. S4B).

The comparison of allosteric interactions in different RyR1 functional states denote that several partial overlapped networks were evident, specifically among the closed $Ca^{2+}$ bound-closed, ATP/CFF bound-closed and $Ca^{2+}$/ATP/CFF bound-closed states (Fig. S2-S6). Furthermore, the interactions that bypassed the ATP- and CFF- binding sites partially overlapped with the network of interactions in $Ca^{2+}$ bound-closed state. Partial alignment of interactions between ATP/CFF bound-closed and $Ca^{2+}$/ATP/CFF bound-closed states emphasize the regulatory role of CFF and ATP in $Ca^{2+}$-dependent RyR1 activation. Further, the binding of ATP and CFF molecules altered the orientation of the CTD and S6c domains and amplified the communication between $Ca^{2+}$ and pore region to modulate pore opening and closing. Hence,

ATP and CFF act as modulators for $Ca^{2+}$ to pore communication and subsequent RyR1 activation.

*ATP- and CFF- binding sites mediate the communication between $Ca^{2+}$- and the pore in $Ca^{2+}$/ATP/CFF bound - open RyR1 structure.*

Three allosteric interactions were predicted to transduce the signal from the $Ca^{2+}$ binding site to the pore region through either CFF or ATP binding sites in $Ca^{2+}$/ATP/CFF bound-open RyR1 structure (PBD ID: 5TAL) (Fig. 5). Two networks of interactions passed through the CFF site initiated from $Ca^{2+}$ binding pocket residue Thr-5001 and proceeded through CTD residues Glu-5002, His-5003, Trp-5011 to Tyr-5014 (Fig. S1). Allosteric communication between the CTD and the TaF domain was propagated through a series of overlapping interactions among the CTD (Tyr-5014) and the S2S3 (Trp-4716, Tyr-4715 and Lys-4675 to Glu-4239) domains. Subsequently, the allosteric signal from the TaF reside Glu-4239 progressed through Phe-4237, Phe-4217, Ile-4218, and S6c residues Val-4950, Gln-4946, Glu-4942 and Asp-4938 to reach the pore region. Hence, in the $Ca^{2+}$/ATP/CFF bound-open RyR1 structure CFF binding site residues Tyr-5014 and Glu-4239 were predicted to propagate the signal between the $Ca^{2+}$ binding site and pore region (Figs. S2B and S5B) by transferring the signal to TaF residues Phe-4237 and Phe-4217. The other connection that passed the signal from the $Ca^{2+}$ binding site to pore through the ATP binding site, instead of the CFF binding site, was predicted to proceed through the CTD residues Thr-5001, Glu-5002, Lys-4998, Tyr-4994, Phe-4991, Tyr-4998, Leu-4985 and S6c residues Met-4954**,** Asp-4953, Val-4950, Gln-4946, Glu-4942, Asp-4938, and Ile-4937. S2S3 residues Tyr-4715 and Phe-4671 and TaF residues Phe-4243, Glu-4244, Ser-4213, and Lys-4214 provided a direct link between the CFF and ATP binding sites. Notably, the communication that

progressed through the S2S3 domain is most dominant due to its strength of interactions and synergistic communication among TaF, S2S3, CTD and pore domains.

High resolution cryo-EM structures (10) revealed that binding of $Ca^{2+}$, ATP, and CFF initiate structural changes in peripheral and central domains associated with transition between open and closed states of RyR1. Fig. 6 as an example provides a visual illustration for the $Ca^{2+}$ binding site to pore communication in closely related primary $Ca^{2+}$/ATP/CFF bound-open and $Ca^{2+}$/ATP/CFF bound-closed structures passing through the CFF binding site, CTD, TaF, and S6c domains encompassing the two allosteric interactions. Specifically, the twisting and outward tilting of the S6c helix from the vertical axis opens up the channel to $Ca^{2+}$ by rotating the Cα atoms of constriction site residues Ile-4937 (closed) and Gln-4933 (open) away from the pore (10, 30).

**Discussion**

The assessment of allosteric interactions between $Ca^{2+}$ binding site and pore region in various RyR1 functional states highlighted structural differences in the organization of activation module. Specifically, the CTD exhibited distinct differences in transducing the effects of $Ca^{2+}$ binding on the ATP or CFF binding sites. The TaF domain residues Phe-4217 and Phe-4237 were identified as part of an allosteric network in all four structures that mediated the signal from the CFF binding site to the pore region. Involvement of the S2S3 domain in transducing the effects of $Ca^{2+}$ to the TaF domain was predicted to be limited to the ATP/CFF bound-closed and $Ca^{2+}$/ATP/CFF bound-open structures. Structural differences in the organization of the CTD and S6c domains in ATP/CFF bound-closed, $Ca^{2+}$/ATP/CFF bound-closed, and $Ca^{2+}$/ATP/CFF bound-open states demonstrate that significant structural changes occur in the activation module

during the $Ca^{2+}$ dependent RyR1 activation. We also predicted major differences in the communication between the ATP and CFF sites in the ATP/CFF bound-closed and $Ca^{2+}$/ATP/CFF bound-closed and -open states. Previous studies showed that the binding of CFF in the presence of an adenine nucleotide altered the orientation of Trp-4716 in the TaF domain and induced conformational changes in CTD to modulate $Ca^{2+}$ binding pocket structure for more favorable binding of $Ca^{2+}$ (19). The subsequent binding of $Ca^{2+}$ initiated reorientation of the CTD and thereby induced flexible alterations in the activation module, which comprises EF1&2, TaF, S2S3, S6c helix, and CTD. The activation module thus acquired a conformation and orientation responsible for pore enlargement as evident from the cryo-EM data of $Ca^{2+}$/ATP/CFF bound-open RyR1 structure (10).

Several amino acid variants in the predicted allosteric interactions were shown to affect RyR1 function. RyR1-T5001A and RyR1-Q3970K in the $Ca^{2+}$ binding site exhibited an altered $Ca^{2+}$-dependent single channel activity, and RyR1-Q3970K displayed reduced activation by CFF or ATP (18, 31). RyR1-W4716A and RyR1-I4996A variants in the CFF-binding pocket of RyR1 and RyR2 increased $Ca^{2+}$ sensitivity in [$^3$H]ryanodine binding ligand assay by controlling the structure of the $Ca^{2+}$ binding site (19). Mutations in the S6c helix such as RyR1 residues Gln-4933, Ile-4937, Asp-4838, Gln-4946, Gln-4947 and Gly-4934 impaired $Ca^{2+}$-gated activity and/or reduced $Ca^{2+}$ conductance (30, 32, 33). Thus, combined impaired $Ca^{2+}$ activation and ion conductance upon mutating pore-lining helix residues suggested allosteric coupling between the $Ca^{2+}$ binding site and pore region.

To summarize, the allosteric interactions among three ligand binding sites and the pore region of RyR1 were investigated in four functional states. The studies predicted that the opening and closing of the pore is allosterically coupled to $Ca^{2+}$, ATP and CFF binding sites and that the

communication between $Ca^{2+}$ binding to pore region is mediated by CFF binding and ATP binding site residues in both open and closed RyR1 structures. Previous studies showed that the addition of ATP and CFF increased channel opening probability in RyR1-WT single channel measurements in the presence and absence of $Ca^{2+}$, and the combined addition of ATP and CFF further increased channel activity. Thus, the enhanced channel opening probability in presence of $Ca^{2+}$, ATP, and CFF suggests allosteric coupling among $Ca^{2+}$, ATP, CFF and the pore region (Fig. 7). Studies in the absence of CFF will provide more direct insights into the allostery mediated by the two physiological activators $Ca^{2+}$ and ATP. An extension to other endogenous ligands such as $Mg^{2+}$ and calmodulin or exogenous effectors may corroborate a complex network of interacting domains and assist in designing therapeutics for skeletal muscle myopathies such as core diseases and malignant hyperthermia or catecholaminergic polymorphic ventricular tachycardia in the heart.

**Author contributions**

Conceived and designed the experiments: VRC, GM, and NVD. Performed the experiments: VRC and KIP. Analyzed the data: VRC. Wrote the paper: VRC, KIP, GM, and NVD.

**Acknowledgements**

We thank Dr. Jian Wang for developing an interactive web server to depict graph-inspired pathways in RyR1. N.V.D. acknowledges NIH support grants R35GM134864 and RO1GM123247. N.V.D. and G.M. are supported by NIH grant AR018687.

**Conflict of interest**

The authors declare no conflicts of interest with the contents of this article.

**References:**


1. Fill, M., and J.A. Copello. 2002. Ryanodine Receptor Calcium Release Channels. *Physiol. Rev.* 82:893–922.
2. Bers, D.M. 2004. Macromolecular complexes regulating cardiac ryanodine receptor function. *J. Mol. Cell. Cardiol.* 37:417–429.
3. Meissner, G. 2017. The structural basis of ryanodine receptor ion channel function. *J. Gen. Physiol.* 149:1065 LP – 1089.
4. Franzini-Armstrong, C., and F. Protasi. 1997. Ryanodine receptors of striated muscles: a complex channel capable of multiple interactions. *Physiol. Rev.* 77:699–729.
5. Van Petegem, F. 2015. Ryanodine Receptors: Allosteric Ion Channel Giants. *J. Mol. Biol.* 427:31–53.
6. Endo, M. 2009. Calcium-Induced Calcium Release in Skeletal Muscle. *Physiol. Rev.* 89:1153–1176.
7. Ríos, E. 2018. Calcium-induced release of calcium in muscle: 50 years of work and the emerging consensus. *J. Gen. Physiol.* 150:521 LP – 537.

8. Bai, X.-C., Z. Yan, J. Wu, Z. Li, and N. Yan. 2016. The Central domain of RyR1 is the transducer for long-range allosteric gating of channel opening. *Cell Res.* 26:995–1006.

9. Wei, R., X. Wang, Y. Zhang, S. Mukherjee, L. Zhang, Q. Chen, X. Huang, S. Jing, C. Liu, S. Li, G. Wang, Y. Xu, S. Zhu, A.J. Williams, F. Sun, and C.-C. Yin. 2016. Structural insights into Ca(2+)-activated long-range allosteric channel gating of RyR1. *Cell Res.* 26:977–994.

10. des Georges, A., O.B. Clarke, R. Zalk, Q. Yuan, K.J. Condon, R.A. Grassucci, W.A. Hendrickson, A.R. Marks, and J. Frank. 2016. Structural Basis for Gating and Activation of RyR1. *Cell*. 167:145-157.e17.

11. Zheng, W. 2015. Toward decrypting the allosteric mechanism of the ryanodine receptor based on coarse-grained structural and dynamic modeling. *Proteins*. 83:2307—2318.

12. Steele, T.W.E., and M. Samsó. 2019. The FKBP12 subunit modifies the long-range allosterism of the ryanodine receptor. *J. Struct. Biol.* 205:180–188.

13. Efremov, R.G., A. Leitner, R. Aebersold, and S. Raunser. 2014. Architecture and conformational switch mechanism of the ryanodine receptor. *Nature*. 517:39.

14. Yan, Z., X. Bai, C. Yan, J. Wu, Z. Li, T. Xie, W. Peng, C. Yin, X. Li, S.H.W. Scheres, Y. Shi, and N. Yan. 2014. Structure of the rabbit ryanodine receptor RyR1 at near-atomic resolution. *Nature*. 517:50.

15. Zalk, R., O.B. Clarke, A. des Georges, R.A. Grassucci, S. Reiken, F. Mancia, W.A. Hendrickson, J. Frank, and A.R. Marks. 2015. Structure of a mammalian ryanodine receptor. *Nature*. 517:44–49.

16. Samsó, M. 2017. A guide to the 3D structure of the ryanodine receptor type 1 by cryoEM. *Protein Sci.* 26:52–68.

17. Dashti, A., G. Mashayekhi, M. Shekhar, D. Ben Hail, S. Salah, P. Schwander, A. des Georges, A. Singharoy, J. Frank, and A. Ourmazd. 2020. Retrieving functional pathways of biomolecules from single-particle snapshots. *Nat. Commun.* 11:4734.

18. Xu, L., V.R. Chirasani, J.S. Carter, D.A. Pasek, N. V Dokholyan, N. Yamaguchi, and G. Meissner. 2018. Ca2+-mediated activation of the skeletal-muscle ryanodine receptor ion channel. *J. Biol. Chem.* . 293:19501–19509.

19. Murayama, T., H. Ogawa, N. Kurebayashi, S. Ohno, M. Horie, and T. Sakurai. 2018. A tryptophan residue in the caffeine-binding site of the ryanodine receptor regulates Ca2+ sensitivity. *Commun. Biol.* 1:98.

20. Dokholyan, N. V. 2016. Controlling Allosteric Networks in Proteins. *Chem. Rev.* 116:6463–6487.

21. Proctor, E.A., P. Kota, A.A. Aleksandrov, L. He, J.R. Riordan, and N. V Dokholyan. 2015. Rational Coupled Dynamics Network Manipulation Rescues Disease-Relevant Mutant Cystic Fibrosis Transmembrane Conductance Regulator. *Chem. Sci.* 6:1237–1246.

22. Dagliyan, O., M. Tarnawski, P.-H. Chu, D. Shirvanyants, I. Schlichting, N. V Dokholyan, and K.M. Hahn. 2016. Engineering extrinsic disorder to control protein activity in living cells. *Science (80-. ).* 354:1441 LP – 1444.

23. Wang, J., A. Jain, L.R. McDonald, C. Gambogi, A.L. Lee, and N. V Dokholyan. 2020. Mapping allosteric communications within individual proteins. *Nat. Commun.* 11:3862.

24. Mei, Y., L. Xu, D.D. Mowrey, R. Mendez Giraldez, Y. Wang, D.A. Pasek, N. V Dokholyan, and G. Meissner. 2015. Channel Gating Dependence on Pore Lining Helix Glycine Residues in Skeletal Muscle Ryanodine Receptor. *J. Biol. Chem.* 290:17535–

17545.

25. Dokholyan, N. V, L. Li, F. Ding, and E.I. Shakhnovich. 2002. Topological determinants of protein folding. *Proc. Natl. Acad. Sci.* 99:8637 LP – 8641.

26. Yen, J.Y. 1971. Finding the K Shortest Loopless Paths in a Network. *Manage. Sci.* 17:712–716.

27. Dijkstra, E.W. 1959. A note on two problems in connexion with graphs. *Numer. Math.* 1:269–271.

28. Suzuki, R., and H. Shimodaira. 2006. Pvclust: an R package for assessing the uncertainty in hierarchical clustering. *Bioinformatics*. 22:1540–1542.

29. The PyMOL Molecular Graphics System, Version 2.0 Schrödinger, LLC. .

30. Mowrey, D.D., L. Xu, Y. Mei, D.A. Pasek, G. Meissner, and N. V Dokholyan. 2017. Ion-pulling simulations provide insights into the mechanisms of channel opening of the skeletal muscle ryanodine receptor. *J. Biol. Chem.* 292:12947–12958.

31. Chirasani, V.R., L. Xu, H.G. Addis, D.A. Pasek, N. V Dokholyan, G. Meissner, and N. Yamaguchi. 2019. A central core disease mutation in the Ca(2+)-binding site of skeletal muscle ryanodine receptor impairs single-channel regulation. *Am. J. Physiol. Cell Physiol.* 317:C358–C365.

32. Xu, L., Y. Wang, D. Gillespie, and G. Meissner. 2006. Two Rings of Negative Charges in the Cytosolic Vestibule of Type-1 Ryanodine Receptor Modulate Ion Fluxes. *Biophys. J.* 90:443–453.

33. Ramachandran, S., A. Chakraborty, L. Xu, Y. Mei, M. Samsó, N. V Dokholyan, and G. Meissner. 2013. Structural Determinants of Skeletal Muscle Ryanodine Receptor Gating. *J. Biol. Chem.* . 288:6154–6165.

**Figure legends**

**Fig. 1. Domain organization and location and structure of ligand binding sites in RyR1 (PDB ID: 5TAL)** (**A)** Co-localization of ATP, CFF, and $Ca^{2+}$ binding sites at interfaces of CTD suggests allosteric communication between these binding sites during channel opening and/or closing. Only two monomers out of four are shown for better visualization of ligand binding sites and RyR1 domains. Protein is shown in cartoon representation and ATP, CFF, and $Ca^{2+}$ are shown in blue, red, and green van der Waals representation, respectively. The important domains of RyR1 that participate in allosteric communication are colored as follows: Core Solenoid (CSol) domain in light blue, EF-hand pair (EF1&2) domain in brown, Thumb and Forefingers (TaF) domain in orange, Helical-bundle domain between S2 and S3 (S2S3) in cyan, Transmembrane domain (TMD) in yellow, Pore domain in magenta, S6c pore helix in green, and Carboxy-terminal domain (CTD) in black. **(B)** Structural conformations of ligand binding sites ($Ca^{2+}$, CFF, and ATP) and pore region of $Ca^{2+}$/ATP/CFF bound-open RyR1 (PDB ID: 5TAL). The side chain of Ile-4937 (constriction site) is shown in licorice to demonstrate the open pore conformation.

**Fig. 2. Allosteric pathway analysis on $Ca^{2+}$ bound-closed RyR1 structure (PDB ID: 5T15).** (A) The network of allosteric connections between $Ca^{2+}$ binding site and pore region in $Ca^{2+}$ bound-closed RyR1 structure. Protein is shown in transparent gray cartoon representation and $Ca^{2+}$ and pore lining residue Gly-4934 as green sphere. The allosteric pathways between $Ca^{2+}$ and

pore regions are shown in red and blue with Cα atoms of allosteric information passing residues (hot spot residues) as gray spheres. (B) Allosteric communication between $Ca^{2+}$ binding site and pore region. Bars corresponding to residues participating in most optimal allosteric pathway between $Ca^{2+}$ binding site and pore region are highlighted in red. Bars for residues participating in other possible but least significant pathways are colored in blue. The height of bars in each chart represents the extent of allosteric information transmitted through the corresponding residue. Inter-residue interactions are rendered as blue cylinders. Color code for RyR1 domains participating in allosteric communication among the ligand sites is as follows: TaF domain (4175–4253) in orange, helical-bundle domain between S2 and S3 (4666–4786) in cyan, channel pore domain (4820–4956) in green, and CTD (4957–5037) in gray. ATP and CFF are shown in green licorice representation, and $Ca^{2+}$ is shown in green van der Waals representation.

**Fig. 3. Mapping allosteric pathways in ATP/CFF bound-closed RyR1 structure (PDB ID: 5TAP).** (A) Network of allosteric connections among ATP and CFF ligand binding sites and pore region in ATP/CFF bound-closed RyR1 structure. Protein is shown in transparent gray cartoon representation, ATP and CFF are shown in green licorice, and pore lining residue Gly-4934 is shown as green sphere. Color code for allosteric pathways shown in this figure is as follows: CFF-pore in red and blue, ATP-pore in orange and blue, and CFF-ATP in cyan. Cα atoms of allosteric information passing residues (hot spot residues) are as gray spheres. (B) Allosteric communications between CFF - pore and ATP - pore regions. Bars corresponding to residues participating in most optimal allosteric pathway between $Ca^{2+}$ binding site and pore region are highlighted in red. Bars for residues participating in other possible but least significant pathways are colored in blue. The height of bars in each chart represents the extent of allosteric information transmitted through the corresponding residue. Inter-residue interactions are rendered as blue cylinders. Color code for RyR1 domains participating in allosteric communication among the ligand sites is as follows: TaF domain (4175–4253) in orange, helical-bundle domain between S2 and S3 (4666–4786) in cyan, channel pore domain (4820–4956) in green, and CTD (4957–5037) in gray. ATP and CFF are shown in green licorice van der Waals representations.

**Fig. 4. Co-regulation interactions in $Ca^{2+}$/ATP/CFF bound-closed RyR1 structure (PDB ID: 5TAQ).** (A) The detailed network of allosteric connections among the three ligand sites (CFF, ATP, and $Ca^{2+}$) and the pore region in $Ca^{2+}$/ATP/CFF bound-closed RyR1 structure. Protein is shown in transparent gray cartoon representation, ATP and CFF are shown in green licorice, and $Ca^{2+}$ and pore lining residue Gly-4934 are as green spheres. Color code for allosteric pathways shown in this figure is as follows: $Ca^{2+}$-pore and $Ca^{2+}$-CFF-pore in red and blue, $Ca^{2+}$-ATP-pore in orange and blue, and CFF-ATP in cyan. Cα atoms of allosteric information passing residues (hot spot residues) are as gray spheres. (B) Allosteric communication between $Ca^{2+}$, ATP and CFF binding sites and pore region. Bars corresponding to residues participating in most optimal allosteric pathway between binding sites and pore region are highlighted in red. Bars for residues participating in other possible but least significant pathways are colored in blue. The height of bars in each chart represents the extent of allosteric information transmitted through the corresponding residue. The interactions between residues participate in allosteric communication between ligand sites are rendered as blue cylinders. Color code for RyR1 domains participating in allosteric communication among the ligand sites is as follows: TaF domain (4175–4253) in orange, Helical-bundle domain between S2 and S3 (4666–4786) in cyan, channel pore domain (4820–4956) in green, and CTD (4957–5037) in gray. ATP and CFF are shown in green licorice representation, and $Ca^{2+}$ is shown in green van der Waals representation.

**Fig. 5. Mapping allosteric pathways in $Ca^{2+}$/ATP/CFF bound-open RyR1 structure (PDB ID: 5TAL).** (A) The detailed network of allosteric connections among the three ligand sites (CFF, ATP, and $Ca^{2+}$) and the pore region in $Ca^{2+}$/ATP/CFF bound-open RyR1 structure. Protein is shown in transparent gray cartoon representation, ATP and CFF are shown in green licorice, and $Ca^{2+}$ and pore lining residue Gly-4934 are as green spheres. Color code for allosteric pathways shown in this figure is as follows: $Ca^{2+}$-pore and $Ca^{2+}$-CFF-pore in red and blue, $Ca^{2+}$-ATP-pore in orange and blue, and CFF-ATP in cyan. Cα atoms of allosteric information passing residues (hot spot residues) are as gray spheres. (B) Allosteric communication between $Ca^{2+}$, ATP and CFF binding sites and pore region. Bars corresponding to residues participating in most optimal allosteric pathway between $Ca^{2+}$ binding site and pore region are highlighted in red. Bars for residues participating in other possible but least significant pathways are colored in blue. The height of bars in each chart represents the extent of allosteric information transmitted through the

corresponding residue. The interactions between residues participate in allosteric communications between ligand sites are rendered as blue cylinders. Color code for RyR1 domains participating in allosteric communication among the ligand sites is as follows: TaF domain (4175–4253) in orange, helical-bundle domain between S2 and S3 (4666–4786) in cyan, channel pore domain (4820–4956) in green, and CTD (4957–5037) in gray. ATP and CFF are shown in green licorice representation, and $Ca^{2+}$ is shown in green van der Waals representation.

**Fig 6. Structural basis of RyR1 channel gating.** Shown is a visual illustration of $Ca^{2+}$ to pore communication in $Ca^{2+}$/ATP/CFF bound - open and $Ca^{2+}$/ATP/CFF bound- closed structures. The structure of open RyR1 is shown in salmon and closed RyR1 in color based on domains for better visualization. The pathway passing through the CFF binding site, CTD (gray), TaF (orange) and S6c (light green) domains encompassing the two allosteric interactions. Ile-4937 and Gln-4933 are the constriction sites of the closed and open channel, respectively. The differential interactions in closed-RyR1 are colored green and corresponding residues are shown in red. Twisting and outward tilting of the S6c helix from the vertical axis opened the channel to $Ca^{2+}$ by rotating the Cα atoms of Ile-4937 and Gln-4933 away from the pore.

**Fig 7. Molecular basis of synergy of channel regulation by multiple activators in closed RyR1.** Schematic representation of residues responsible for initiating allosteric signal from each ligand-binding site and residues that modulate and propagate the allosteric communication to the pore region. Ile-4937 obstructs ion conductance in closed RyR1.

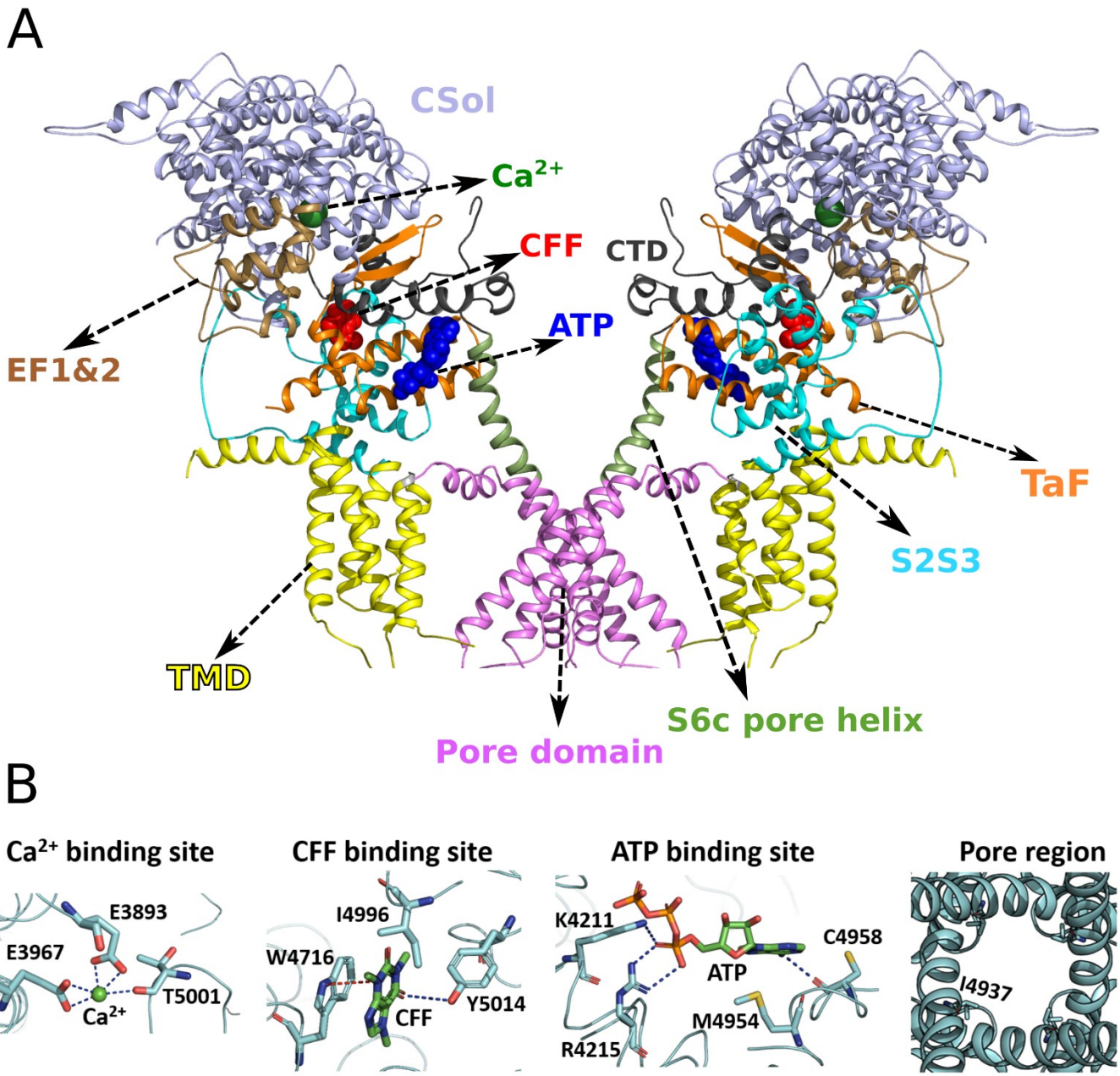
A
CSol
Ca2+
CFF
CTD
ATP
EF1&2
TaF
S2S3
TMD
S6c pore helix
Pore domain
B
Ca2+ binding site
E3893
E3967
T5001
Ca2+
CFF binding site
I4996
W4716
CFF
Y5014
ATP binding site
K4211
C4958
ATP
M4954
R4215
Pore region
I4937

Figure 1

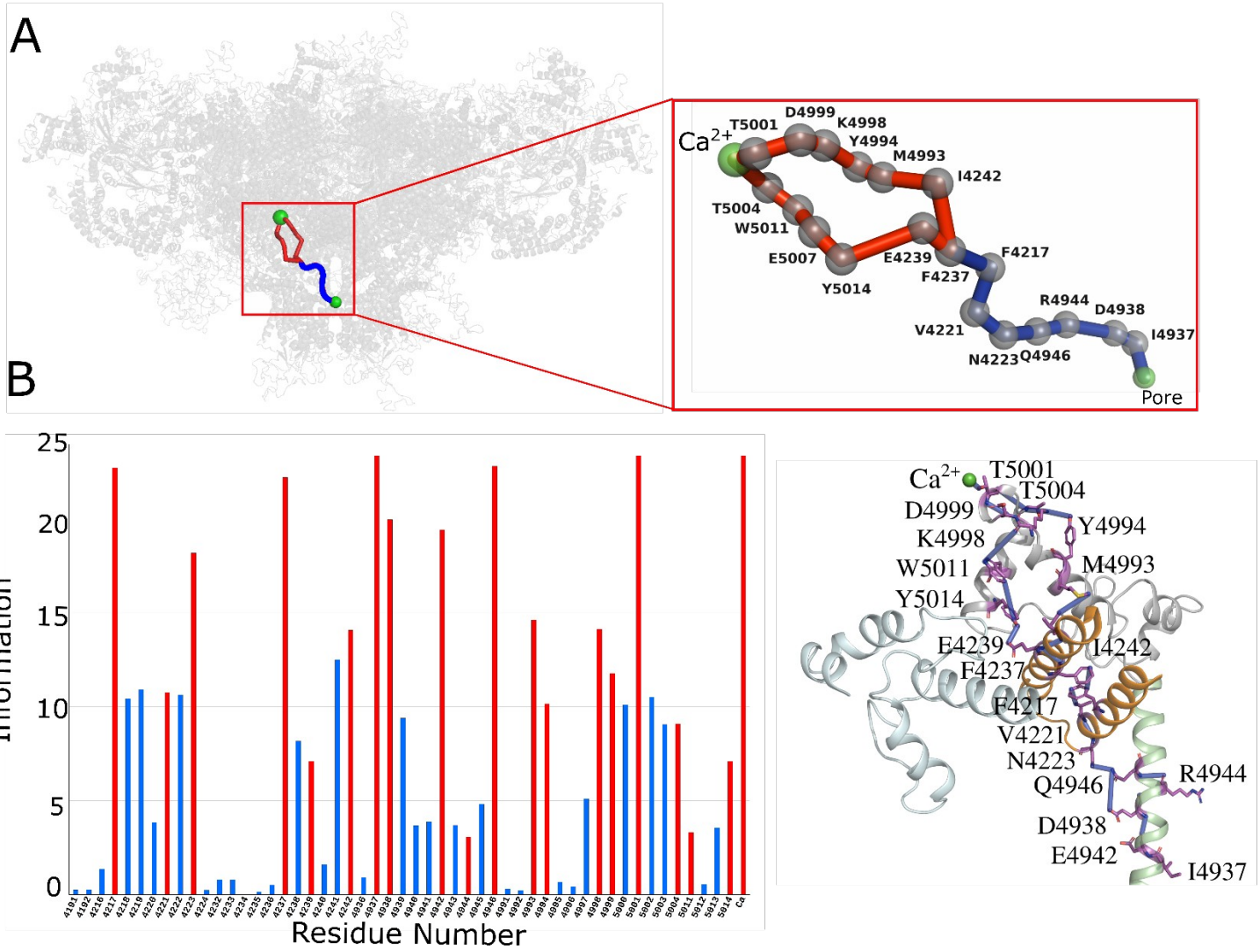
A
B
Ca2+
T5001
D4999
K4998
Y4994
M4993
I4242
T5004
W5011
E5007
E4239
F4217
F4237
Y5014
R4944
D4938
V4221
I4937
N4223
Q4946
Pore
Information
Residue Number
Ca2+
T5001
T5004
D4999
Y4994
K4998
W5011
M4993
Y5014
E4239
I4242
F4237
F4217
V4221
N4223
R4944
Q4946
D4938
E4942
I4937

Figure 2

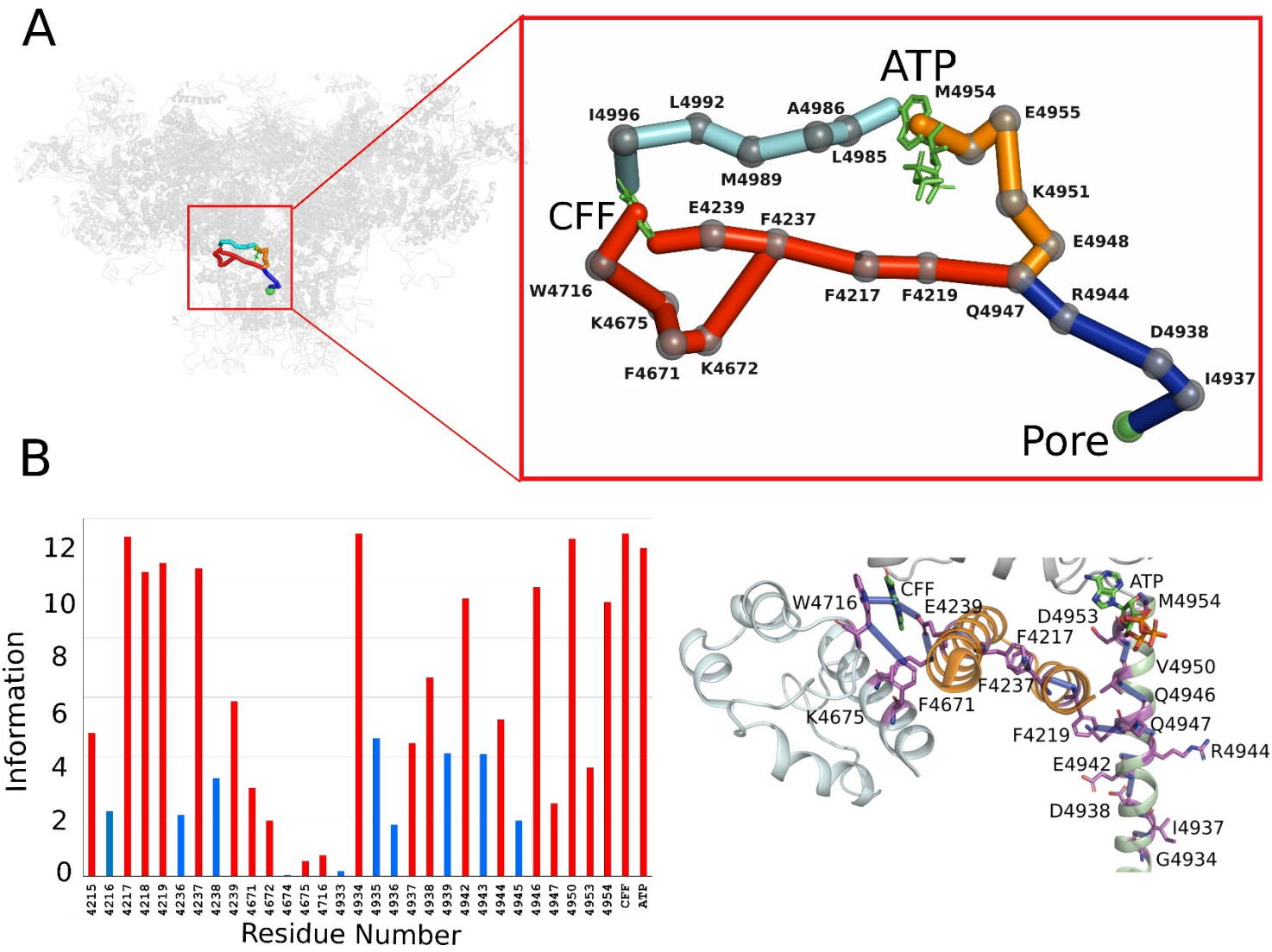
A
ATP
M4954
I4996
L4992
A4986
E4955
L4985
M4989
K4951
CFF
E4239
F4237
E4948
W4716
F4217
F4219
R4944
Q4947
K4675
D4938
F4671
K4672
I4937
Pore
B
Information
12
10
8
6
4
2
0
4215 4216 4217 4218 4219 4236 4237 4238 4239 4671 4672 4674 4675 4716 4933 4934 4935 4936 4937 4938 4939 4942 4943 4944 4945 4946 4947 4950 4953 4954 CFF ATP
Residue Number
CFF
ATP
W4716
E4239
M4954
D4953
F4217
V4950
F4237
Q4946
K4675
F4671
Q4947
F4219
R4944
E4942
D4938
I4937
G4934

Figure 3

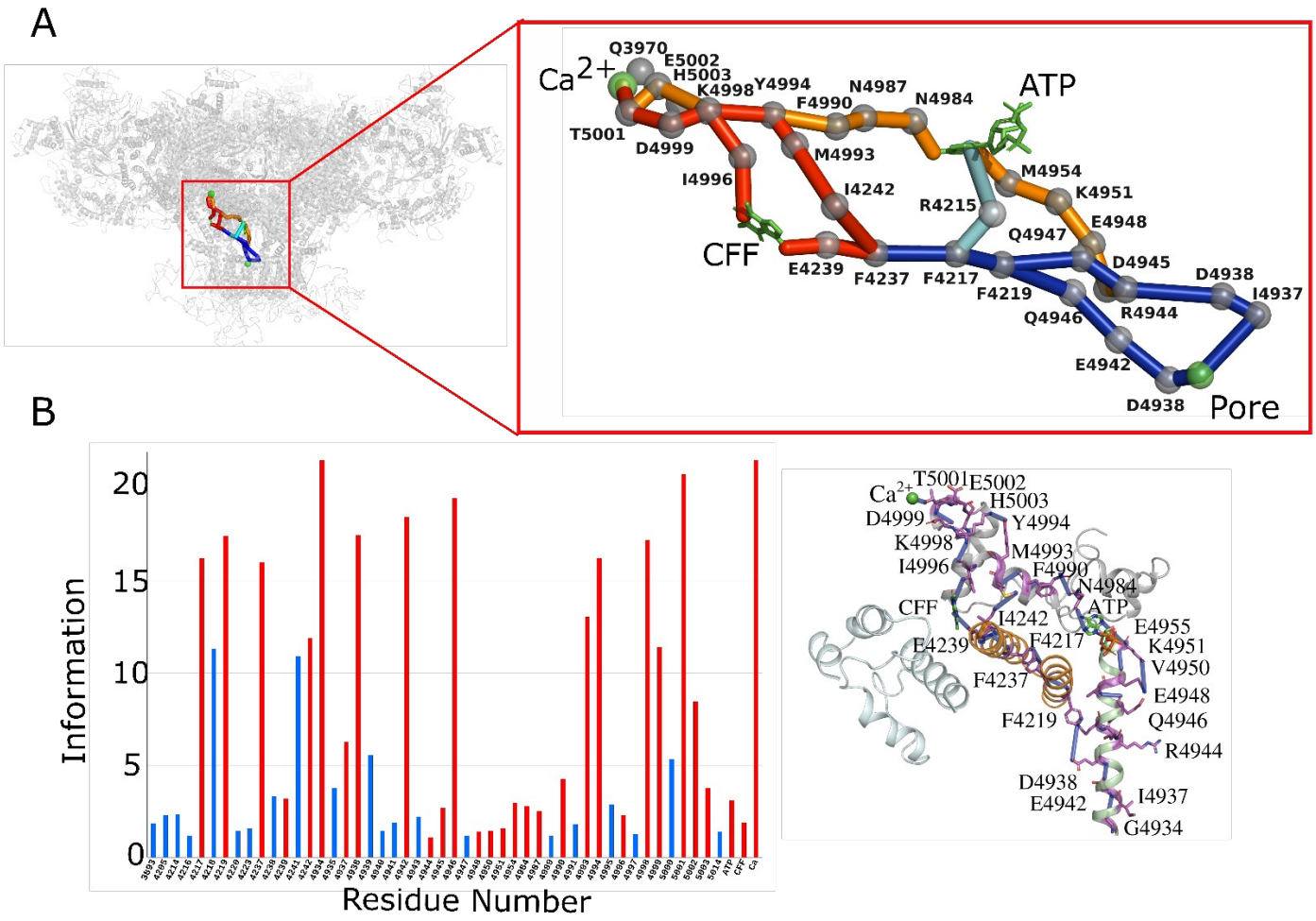
A
Ca2+
Q3970
E5002
H5003
K4998
Y4994
F4990
N4987
N4984
ATP
T5001
D4999
M4993
I4996
I4242
M4954
K4951
R4215
E4948
Q4947
CFF
E4239
F4237
F4217
D4945
D4938
F4219
I4937
Q4946
R4944
E4942
D4938
Pore
B
Information
Residue Number
Ca2+
T5001
E5002
H5003
D4999
Y4994
K4998
M4993
I4996
F4990
N4984
CFF
ATP
I4242
E4955
E4239
F4217
K4951
V4950
F4237
E4948
F4219
Q4946
R4944
D4938
E4942
I4937
G4934

Figure 4

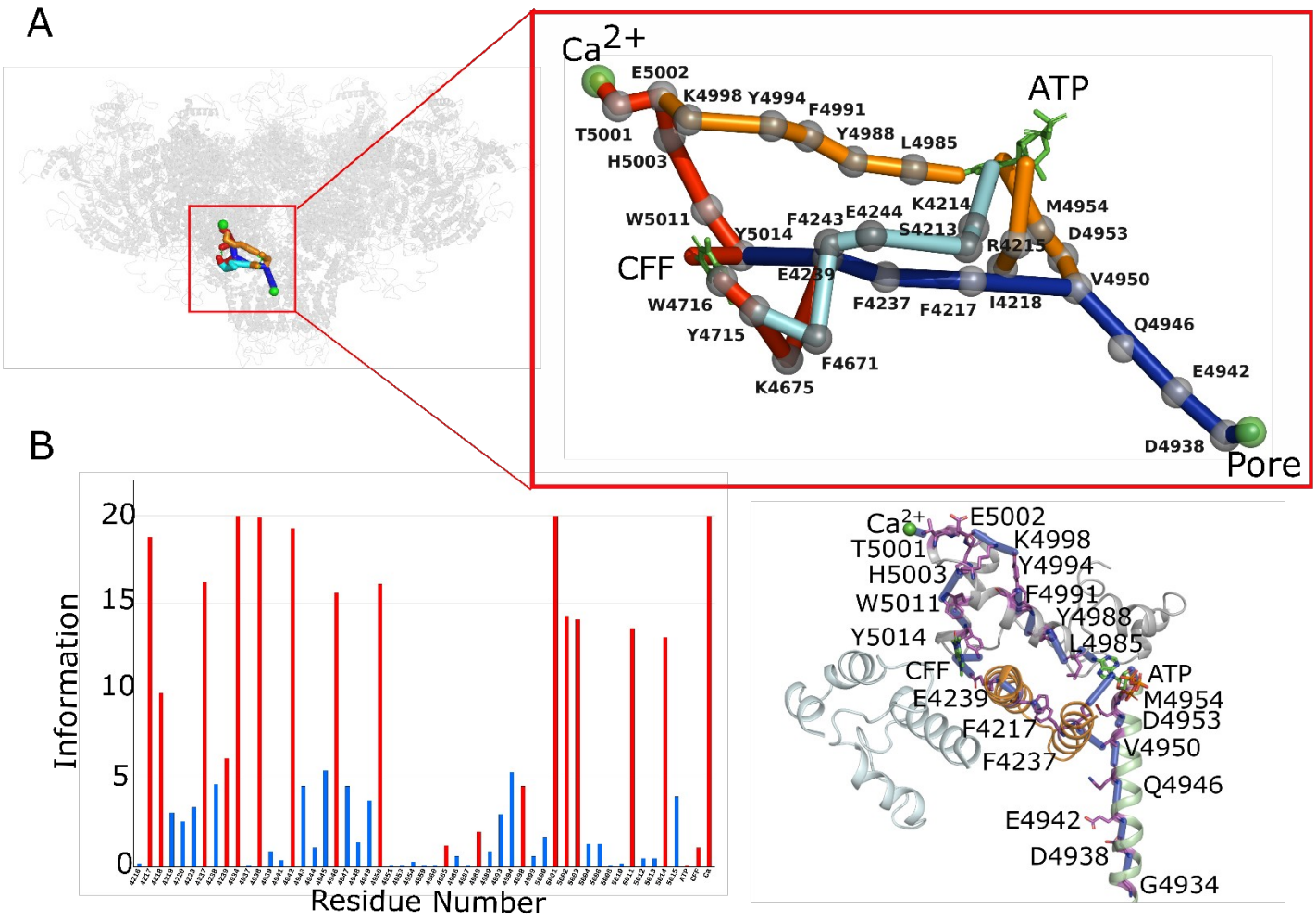
A
Ca2+
E5002
K4998
Y4994
F4991
ATP
T5001
Y4988
L4985
H5003
W5011
F4243
E4244
K4214
M4954
Y5014
S4213
D4953
CFF
R4215
E4239
V4950
W4716
F4237
F4217
I4218
Q4946
Y4715
F4671
E4942
K4675
D4938
Pore
B
Information
Residue Number
Ca2+
E5002
T5001
K4998
H5003
Y4994
W5011
F4991
Y4988
Y5014
L4985
CFF
ATP
E4239
M4954
F4217
D4953
V4950
F4237
Q4946
E4942
D4938
G4934

Figure 5

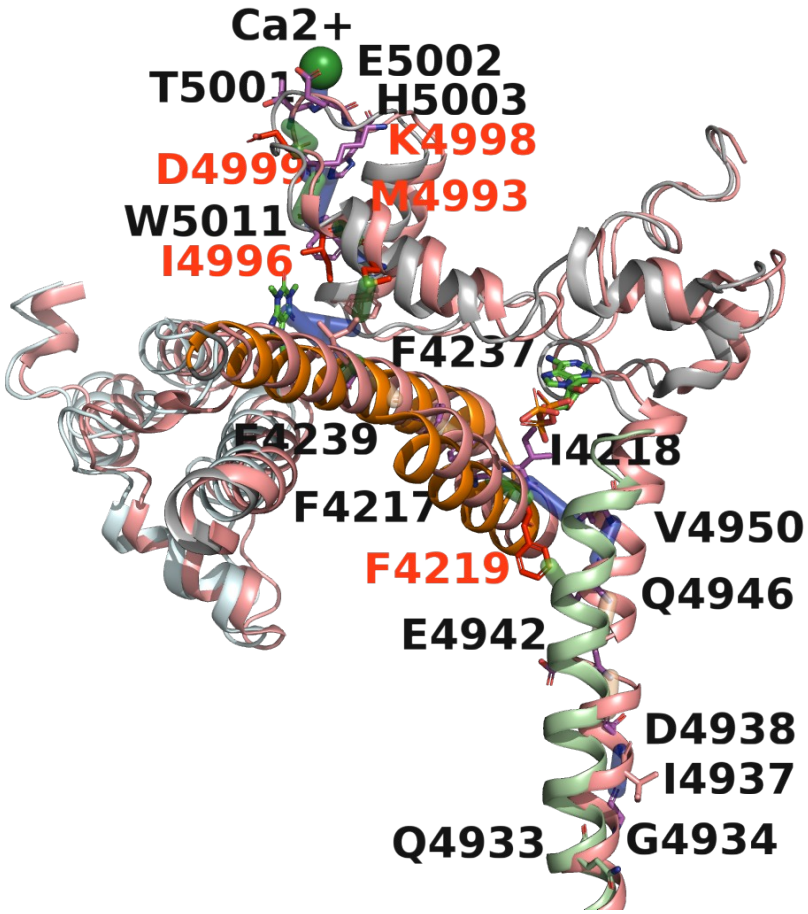
Ca2+
E5002
T5001
H5003
K4998
D4999
M4993
W5011
I4996
F4237
F4239
I4218
F4217
V4950
F4219
Q4946
E4942
D4938
I4937
Q4933
G4934

Figure 6

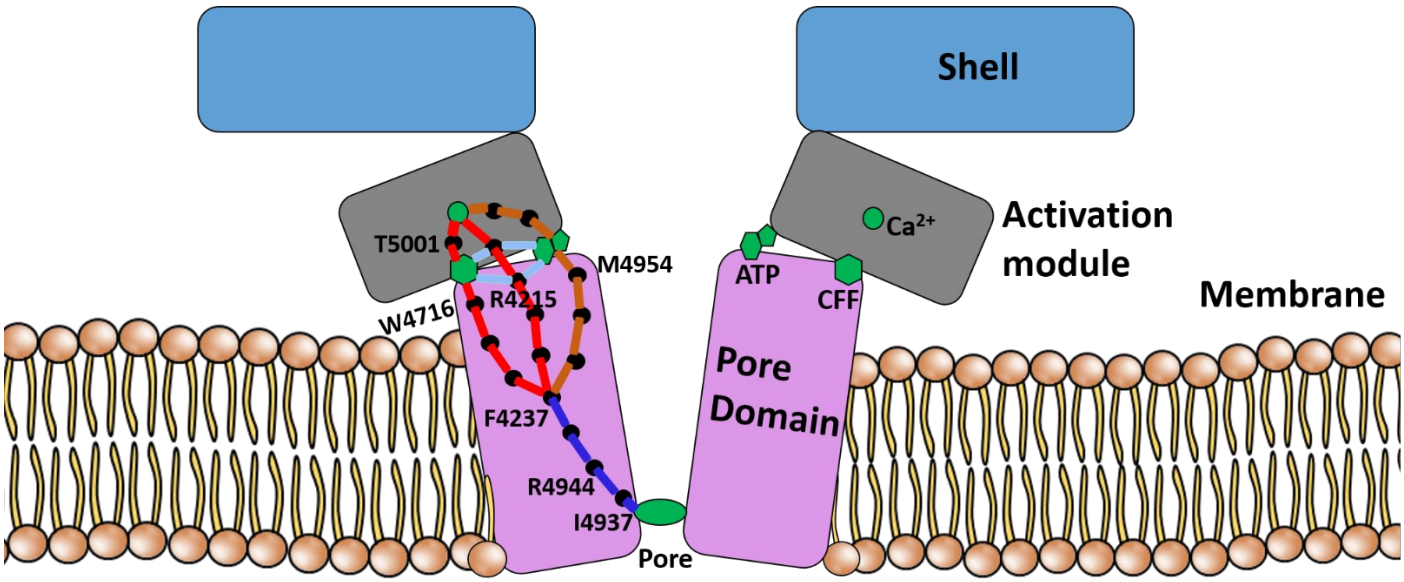
Shell
Activation module
Membrane
T5001
M4954
W4716
R4215
ATP
CFF
Pore Domain
F4237
R4944
I4937
Pore

Figure 7